

Production and constraints of massive dark photon in electron-positron colliders

Jun Jiang ^{a *}, Chun-Yuan Li ^{a †}, Shi-Yuan Li ^{a ‡}, Shankar Dayal Pathak ^{a,b §},
Zong-Guo Si ^{a ¶}, Xing-Hua Yang ^{a ||}

^aSchool of Physics, Shandong University, Jinan, Shandong 250100, China

^b Department of Physics, Lovely Professional University, Phagwara, Punjab, 144411, India

Abstract

Dark sectors may couple to the Standard Model via one or more mediator particles. In this paper, we discuss two types of mediators: the dark photon A' and the dark scalar mediator ϕ . The total cross sections and various differential distributions of signal processes of $e^+e^- \rightarrow q\bar{q}A'$ and $e^+e^- \rightarrow q\bar{q}\phi$ ($q = u, d, c, s$ and b quarks) are discussed, and then we focus on an invisible A' study due to the cleaner background processes at future e^+e^- colliders. It is found that kinematic distributions of the two-jet system can be used to identify or exclude the dark photon and dark scalar mediator, as well as distinguish between them. We further study the possibility of the search for dark photon at future CEPC experiment with $\sqrt{s} = 91.2$ GeV and 240 GeV. Running at $\sqrt{s} = 91.2$ GeV, it is possible for CEPC to perform a decisive measurement on dark photon ($20 \text{ GeV} < m_{A'} < 60 \text{ GeV}$) in less than one operating year. The lower limits of integrated luminosity for significance $S/\sqrt{B} = 2\sigma, 3\sigma$ and 5σ are presented.

1 Introduction

The signals of non-baryonic dark matter (DM) in the universe have been supported by a bunch of astrophysical and cosmological observations, such as the Cosmic Microwave Background anisotropy measurements, galactic rotation curves, large scale structure surveys, X-ray observations and gravitational lensing [1–11]. The contribution of DM is nearly 75% of the total matter in the universe. Specifically, the Planck observational data has given the value of relic density of DM $\Omega_{CDM}h^2 = 0.120 \pm 0.001$ [1]. It shows dynamical effects from galaxy up to cosmic scales and plays a crucial role in galaxy rotation curve and structure formation in the universe. However, the nature of the DM particles remains mysterious and has become one of the most appealing open challenges for modern science. To analyze and investigate the underlying physics of DM particles, there are various worldwide projects working on the DM detection, such as direct and indirect searches, collider experiments and astrophysical signatures arising from DM self-interactions [12–15].

*E-mail: jiangjun87@sdu.edu.cn

†E-mail: lichunyuan@mail.sdu.edu.cn

‡E-mail: lishy@sdu.edu.cn

§E-mail: prince.pathak19@gmail.com

¶E-mail: zgzi@sdu.edu.cn

||E-mail: yangxh@mail.sdu.edu.cn

Given the intricate structure of the Standard Model (SM), which describes only a sub-dominant component of the universe, it would not be too surprising if the dark sector contains a rich structure itself, with DM making up parts of it. In the dark sector, the DM particles do not interact directly to the known strong, weak and electromagnetic forces except for gravitational force. However, there is typically one or more mediator particles which are coupled with SM as the “portal” [16–21]. Such extended interactions associating dark sector and SM depend on the spin and parity: mediators can be vector A' , scalar ϕ , pseudoscalar a , axial-vector Z' and even fermions N .

A new force mediated by dark photons has a subject of deep interest in the high energy particle physics. The existence of the dark photon [22–24], associated to a hidden $U(1)'$ gauge interaction, has been the object of many investigations, both theoretically and experimentally. Substantial efforts have been put by several authors into the search for a dark photon through various processes including bremsstrahlung process $e^-Z \rightarrow e^-ZA'$ [25–28], meson decays process $\pi^0/\eta/\eta' \rightarrow \gamma A'$, $K \rightarrow \pi A'$, $\phi \rightarrow \eta A'$ and $D^* \rightarrow D^0 A'$ [29–31], Drell-Yan process $q\bar{q} \rightarrow A' \rightarrow (\ell^+\ell^- \text{ or } h^+h^-)$ [32,33], annihilation process $e^+e^- \rightarrow \gamma A'$ [34–38], etc., and physicists have obtained stringent limits of the kinetic mixing parameter ε for a given dark photon mass $m_{A'}$ [17,18,24,39,40]. For $m_{A'} \lesssim 1$ GeV, only limited values of ε are allowed. For the heavy massive dark photon, a wide range is still not excluded by current ongoing experiments.

The future high energy electron-positron colliders can provide an opportunity to search for the dark sector mediators. This kind of colliders include CEPC [41], ILC [42], FCC-ee [43] and CLIC [44] with the center-of-energy \sqrt{s} varying from 91.2 GeV to 1 TeV. In this paper, assuming that dark mediators interact only with quarks, we investigate the production of dark photon A' and dark scalar mediator ϕ at electron-positron colliders with $\sqrt{s} = 91.2$ GeV, 240 GeV, 500 GeV and 1 TeV. We analyze the cross sections and the normalized kinematic distributions for the processes of both $e^+e^- \rightarrow q\bar{q}A'$ and $e^+e^- \rightarrow q\bar{q}\phi$, and then we focus on an invisible A' study due to the cleaner background. The corresponding background processes are also simulated.

This paper is organized as follows. In Section 2, we present the simple theoretical framework of dark photon and dark scalar mediator. In Section 3, we investigate the production properties of dark photon and dark scalar mediator at future e^+e^- colliders, and we also discuss how to distinguish between them. In Section 4, we study the discovery potential of the dark photon at the CEPC experiment. Finally a short summary is given.

2 The dark photon and the dark scalar mediators

In the simple extension of SM, one can introduce a $U(1)'$ as an extra gauge group. Then the gauge boson A' arises from the extra $U(1)'$ gauge group, which can be coupled weakly to electrically charged particles through “kinetic mixing” with the photon [22–24]. Kinetic mixing produces an effective parity-conserving interaction $\varepsilon e A'_\mu J_{EM}^\mu$ of the A' to the electromagnetic current J_{EM}^μ , suppressed relative to the electron charge by the parameter ε [18]. The gauge boson or dark photon A' can play the role of “vector portal” connecting the SM and DM particles, we assume that the dark photon only interacts with DM particles and SM quarks. After the kinetic mixing

term diagonalization, the Lagrangian of the dark photon model is [19, 21]

$$\mathcal{L} \supset \sum_q \bar{q}(-ec_q\gamma^\mu A_\mu - \varepsilon ec_q\gamma^\mu A'_\mu - m_q)q + \bar{\chi}(-g_\chi\gamma^\mu A'_\mu - m_{DM})\chi - \frac{1}{4}F_{\mu\nu}F^{\mu\nu} - \frac{1}{4}F'_{\mu\nu}F'^{\mu\nu} + \frac{1}{2}m_{A'}^2 A'^2, \quad (1)$$

where m_q , m_χ and $m_{A'}$ denote the masses of the SM quarks, DM particle and the dark photon respectively. c_q is the charge of the quarks. $F^{\mu\nu}$ and $F'^{\mu\nu}$ are the field strengths of the ordinary photon A and the dark photon A' respectively, ε is the kinetic mixing parameter in the physical basis, g_χ is the coupling parameter between the dark photon and the dark sector and $\alpha_\chi = g_\chi^2/(4\pi)$ is the dark fine structure constant.

A number of experiments have proposed some restrictions on the mixing parameter ε [17, 18, 24, 39]. However, for the massive dark photon with mass of $m_{A'} > 1$ GeV, a wide range is still not excluded by current experiments. We can extract the maximum value of ε from DM direct detection experiments, and the differential cross sections for DM particle-nucleon scattering at the non-relativistic limit can be written as [24, 45, 46]

$$\frac{d\sigma}{dE_R}(v_{DM}, E_R) = \frac{8\pi\alpha_{em}\alpha_\chi\varepsilon^2 m_T}{(2m_T E_R + m_{A'}^2)^2} \frac{1}{v_{DM}} Z_T^2 F^2(2m_T E_R), \quad (2)$$

where E_R is the nuclear recoil energy, v_{DM} is the velocity of the DM particle in the nucleon rest frame, $\alpha_{em} = e^2/4\pi$ is the electromagnetic fine structure constant, m_T is the mass of the target nucleus, Z_T is the number of protons in the target nuclei, and $F(2m_T E_R)$ is the Helm form factor [47, 48]. The dark fine structure constant α_χ can be determined by the relic abundance of DM. When m_χ is determined, we can constrain the combined coupling parameter $\alpha_\chi\varepsilon^2$ from the experimental data through evaluating the function $\chi^2 = -\sum 2\ln\mathcal{L}'$ with \mathcal{L}' being the likelihood function [49, 50]. Fig. 1 shows the 90% C.L. upper limits of the combined parameter $\alpha_\chi\varepsilon^2$ with $m_\chi = 8.6$ GeV (CDMS-II-Si favors a DM mass of $m_\chi \sim 8.6$ GeV [51]) and $m_\chi = 100$ GeV constrained by the CDEX-10 [52], PandaX-II [53], DarkSide-50 [54] and XENON-1T [55] data.

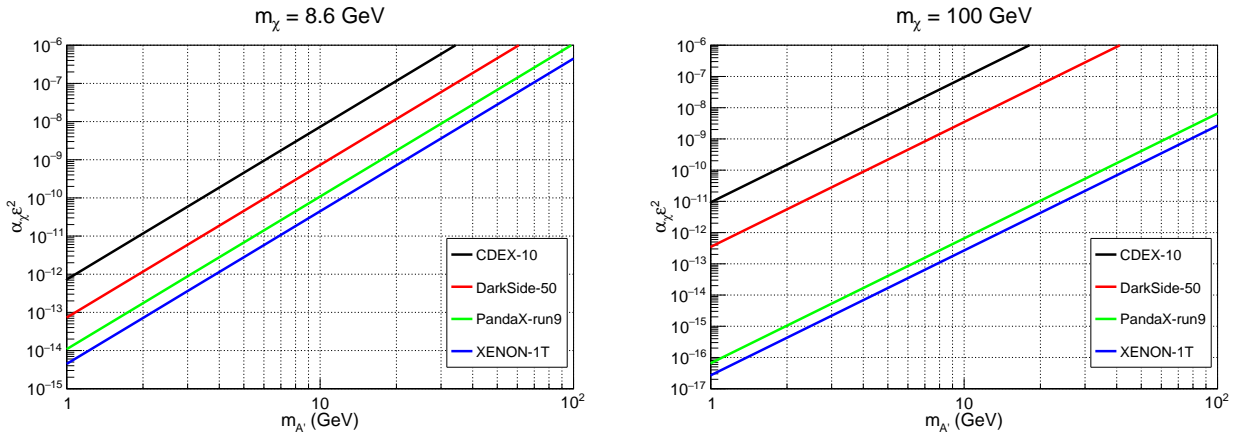


Figure 1: The 90% C.L. upper limits of the combined parameter $\alpha_\chi\varepsilon^2$ with $m_\chi = 8.6$ GeV (left panel) and 100 GeV (right panel) from CDEX-10 [52], PandaX-II [53], DarkSide-50 [54] and XENON-1T [55] experiments.

Alternatively, in dark scalar mediator ϕ model, the DM particles χ can interact with the SM particles through a “Higgs portal” [19, 20]. The corresponding Lagrangian can be written as,

$$\begin{aligned}\mathcal{L} \supset & \frac{1}{2}(\partial_\mu\phi)^2 - \frac{1}{2}m_\phi^2\phi^2 + \bar{\chi}(i\partial_\mu\gamma_\mu - m_\chi - \lambda_\chi\phi)\chi \\ & - \lambda_1 v\phi(H^+H - \frac{v^2}{2}) - \lambda_2\phi^2(H^+H - \frac{v^2}{2}) - V(\phi),\end{aligned}\quad (3)$$

where H is the SM higgs doublet, v is the corresponding vacuum expectation value, and $\lambda_\chi, \lambda_1, \lambda_2$ are three parameters. In the case that $\langle\phi\rangle = 0$ and $\lambda_2 \rightarrow 0$, after electroweak symmetry breaking, the relevant DM and mediator Lagrangian then takes the following form,

$$\mathcal{L} \supset \frac{1}{2}(\partial_\mu\phi)^2 - \frac{1}{2}m_\phi^2\phi^2 + \bar{\chi}(i\partial_\mu\gamma_\mu - m_\chi - \lambda_\chi\phi)\chi - \lambda_1 v^2\phi h, \quad (4)$$

where the interaction between SM particles and DM particles are mediated by Higgs-Singlet mixing, i.e., the $h - \phi$ scalar exchange. In this paper, we assume that the dark scalar mediator ϕ directly couples to the SM quarks q . The dark scalar mediator plays the crucial role in “scalar portal”. Then the mixing term can be written as $-\varepsilon_s e\phi q\bar{q}$. In this work, we choose $\varepsilon_s = \varepsilon$ for simplicity.

3 Production of dark photon and dark scalar mediator

In this section, we investigate the production of the massive dark photon A' and of the massive dark scalar mediator ϕ via the processes $e^+e^- \rightarrow q\bar{q}A'$ and $e^+e^- \rightarrow q\bar{q}\phi$ ($q = u, d, s, c$ and b) at the center-of-mass energy $\sqrt{s} = 91.2$ GeV, 240 GeV, 500 GeV and 1 TeV, with different values of $m_{A'}$ and m_ϕ . The Feynman diagrams for the production of A' and ϕ associated with two jets at e^+e^- colliders are shown in Fig. 2.

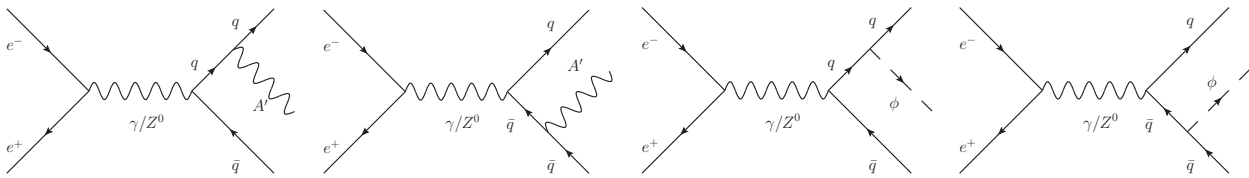


Figure 2: The Feynman diagrams of processes $e^+e^- \rightarrow q\bar{q}A'$ and $e^+e^- \rightarrow q\bar{q}\phi$.

To obtain the analytical amplitudes, we use FeynArts [56] and FeynCalc [57] to generate Feynman diagrams and to make mathematical calculation. We use the multidimensional numerical integration package Cuba [58] to analyze the kinematic distributions. The cross sections of the signal process $e^+e^- \rightarrow q\bar{q}A'$ ($e^+e^- \rightarrow q\bar{q}\phi$) are suppressed by the factors of ε^2 (ε_s^2). In order to consider the general situation, we show the reduced cross sections of the two signal processes with respect to \sqrt{s} and $m_{A'}$ or m_ϕ in Fig. 3. Fig. 3 (a) and (b) exhibit peaks due to the contribution from the resonant Z^0 boson production. Taking $m_{A'} = 20$ GeV as an example, the cross sections decrease by about three orders of magnitude when \sqrt{s} increases from 91.2 GeV to 1 TeV. Fig. 3 (c) and (d) show that the reduced cross sections become smaller as the mass becomes larger. It is worth noting that since values of the coupling parameters ε (ε_s) vary with respect to the masses

$m_{A'}$ (m_ϕ), the line shapes of cross sections with respect to $m_{A'}$ (m_ϕ) will change when adopting the mass-dependent ε (ε_s) inputs. In this paper, we focus on the invisible dark photon A' and dark scalar mediator ϕ production at e^+e^- collider, one can identify them by the reconstruction of the missing momentum, i.e., the recoil of two final jets. Then the four-momentum of two-jet system is used to infer the characteristics of the two processes. Fig. 4 shows the normalized

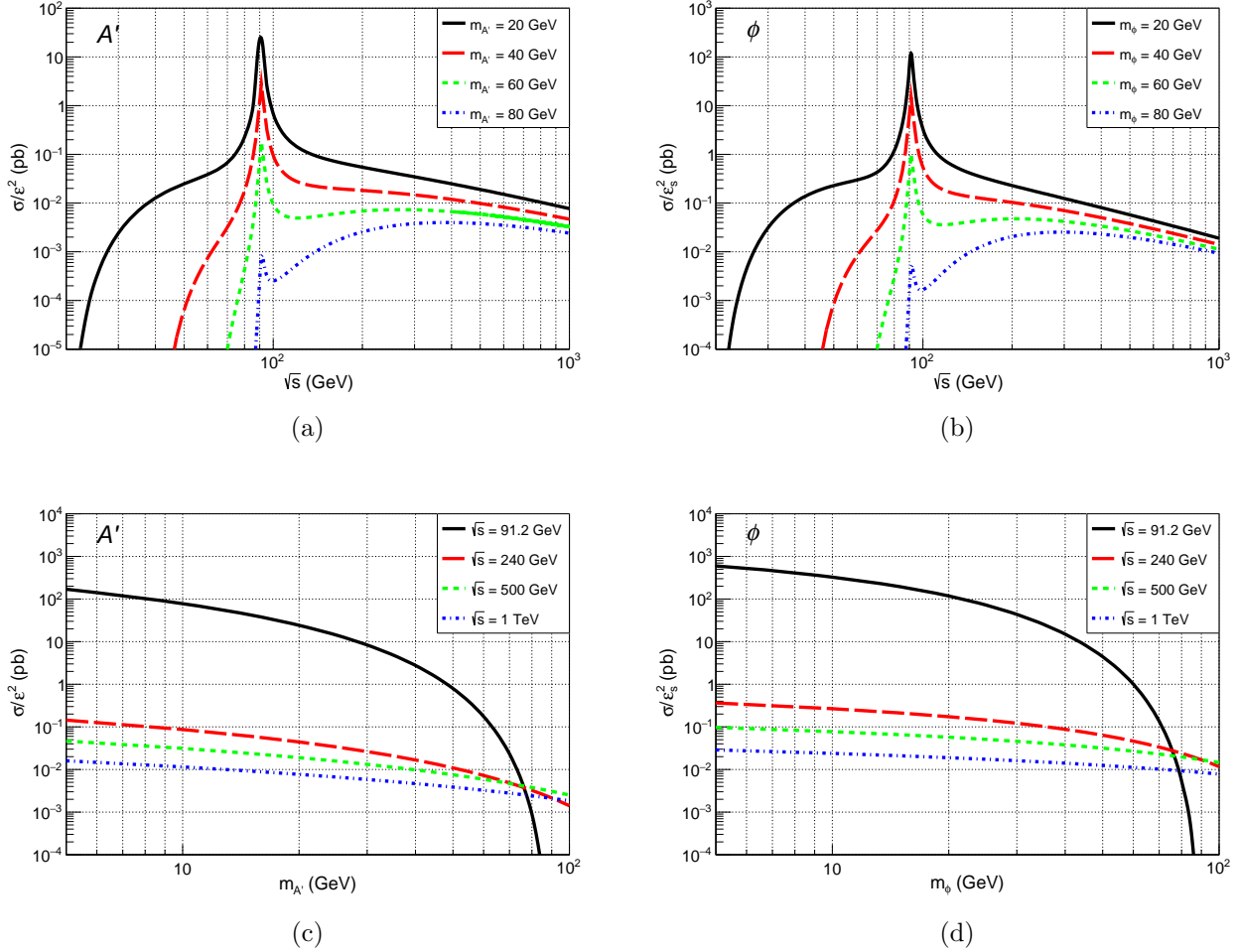


Figure 3: The reduced cross sections of the two processes $e^+e^- \rightarrow q\bar{q}A'$ (left panels) and $e^+e^- \rightarrow q\bar{q}\phi$ (right panels) with respect to \sqrt{s} and $m_{A'}$ or m_ϕ .

P_T^{jj} , M_{jj} , $\cos\theta_{jj-z}$ and η_{jj} distributions of the two-jet system for the two signal processes of $e^+e^- \rightarrow q\bar{q}A'$ (left panels) and $e^+e^- \rightarrow q\bar{q}\phi$ (middle panels) with different \sqrt{s} and $m_{A'}$ (m_ϕ) without any kinematic cuts. Here the P_T^{jj} is the transverse momentum of the two-jet system, M_{jj} is the invariant mass of the two-jet system, θ_{jj-z} is the angle between the momentum of the two-jet system and the particle beam axis, and η_{jj} is the rapidity of the two-jet system. For comparison, we use MadGraph [59] to analyze the kinematic distributions of the dominant background process $e^+e^- \rightarrow q\bar{q}\nu\bar{\nu}$ ($\nu = \nu_e, \nu_\mu$ and ν_τ), which is shown in Fig. 4 (right panels). For $\sqrt{s} \geq 240$ GeV, the M_{jj} distributions of background exhibit two peaks around $M_{jj} \approx 91$ GeV and 125 GeV due to the contributions of the resonant Z^0 and Higgs boson. But for $\sqrt{s} = 91.2$ GeV, the Z^0 peak is not obvious, because we set the minimum transverse momentum of the jets as 0.5 GeV. In

Fig. 4, one can find that the kinematic distributions of the two signal processes are different but not obvious. Then we further investigate the distributions related to both $\cos\theta_{jj-z}$ and P_T^{jj} of the two signal processes in Fig. 5 with different \sqrt{s} and $m_{A'}$ (m_ϕ) values. In comparison with the scalar case, distributions for the dark photon A' signal process are restricted in a smaller area. For example, at $\sqrt{s} = 91.2$ GeV the dominated area for A' signal process is located at $\cos\theta_{jj-z} \in (-1, -0.9)$ and $(0.9, 1)$ with $P_T^{jj} \in (0, 10)$, while dominated districts for ϕ process are comparatively broader. And the higher the center-of-mass energy \sqrt{s} is, the more obvious this trend becomes.

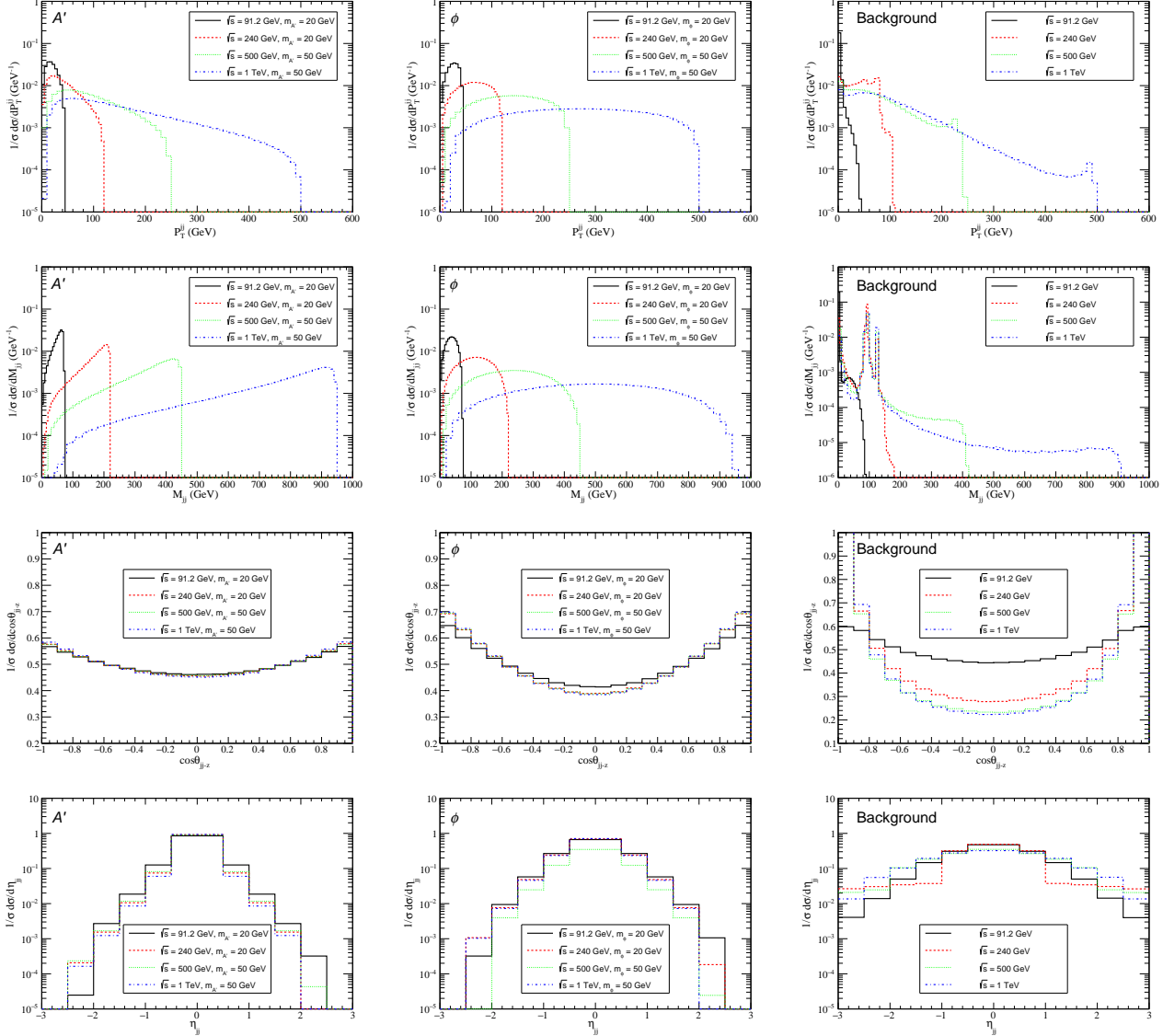


Figure 4: The normalized P_T^{jj} , M_{jj} , $\cos\theta_{jj-z}$ and η_{jj} distributions of the two-jet system for the dark photon production process $e^+e^- \rightarrow q\bar{q}A'$ (left panels), the dark scalar mediator production process $e^+e^- \rightarrow q\bar{q}\phi$ (middle panels) and the dominant background process $e^+e^- \rightarrow q\bar{q}\nu\bar{\nu}$ (right panels) at $\sqrt{s} = 91.2$ GeV, 240 GeV, 500 GeV, and 1 TeV.

As discussed above, some kinematic distributions for dark photon A' and dark scalar mediator ϕ are different. And these different phenomena can be enhanced by imposing proper kinematic cuts.

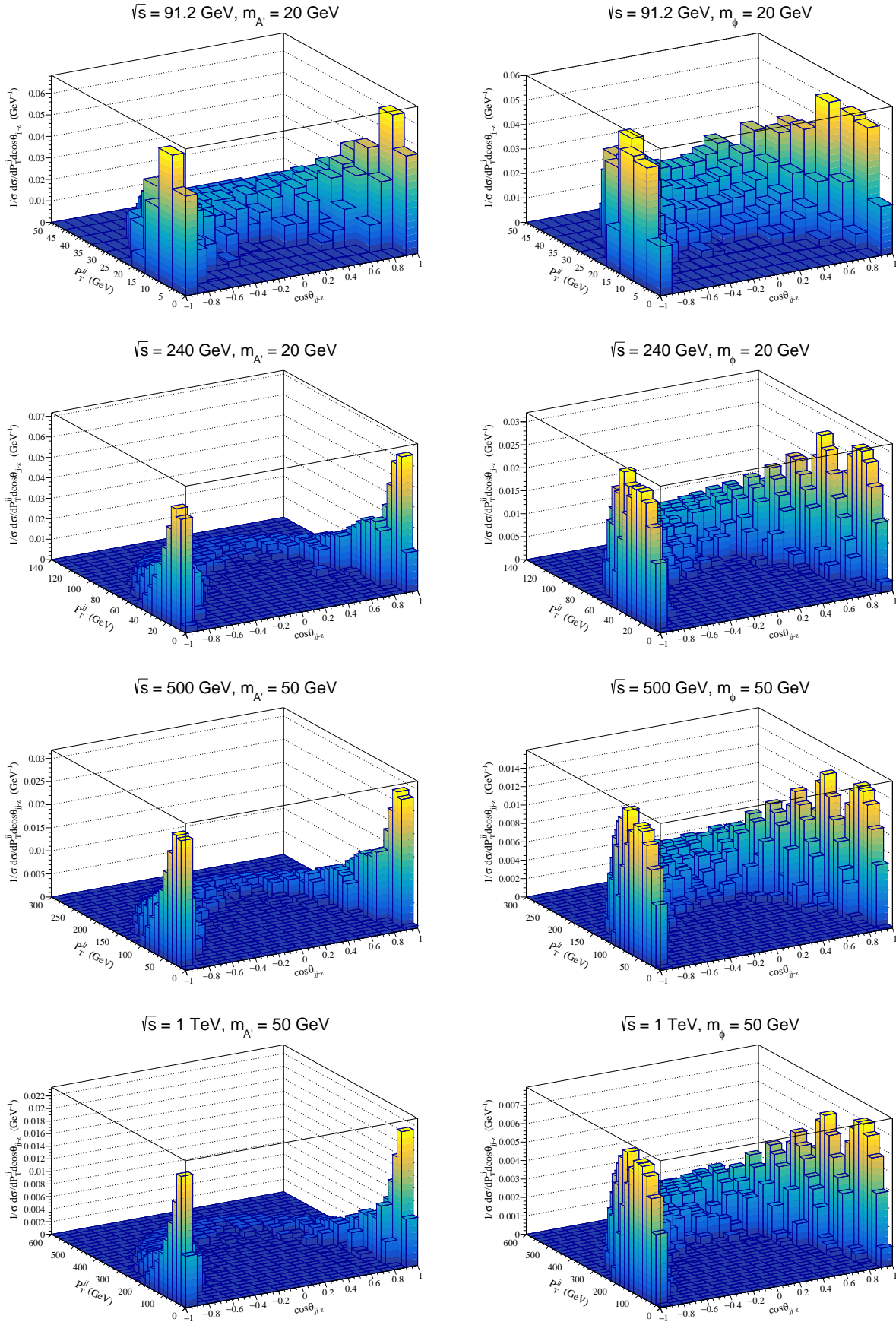


Figure 5: The normalized distributions related to both $\cos\theta_{jj-z}$ and P_T^{jj} for the signal processes $e^+e^- \rightarrow q\bar{q}A'$ (left panels) and $e^+e^- \rightarrow q\bar{q}\phi$ (right panels) with different \sqrt{s} and $m_{A'}$ (m_ϕ) values without any kinematic cuts.

Here, we emphasize on the P_T^{jj} and $\cos\theta_{jj-z}$ distributions of the two signal processes. According to our study below, one can find there exists significant differences between dark photon and dark scalar mediator production at e^+e^- colliders.

In order to show the difference related to P_T^{jj} , we impose a cut on $\cos\theta_{jj-z}$, i.e., $-0.9 < \cos\theta_{jj-z} < 0.9$ as presented in Fig. 6. In the case of $\sqrt{s} = 91.2$ GeV and $m_{A'}(m_\phi) = 20$ GeV, when $18 \lesssim P_T^{jj} \lesssim 40$, the P_T^{jj} distributions of the process $e^+e^- \rightarrow q\bar{q}A'$ are attenuated as P_T^{jj} increases, while the P_T^{jj} distributions of the process $e^+e^- \rightarrow q\bar{q}\phi$ are substantially flat in this region. In the case of $\sqrt{s} = 1$ TeV and $m_{A'}(m_\phi) = 50$ GeV, the differences of P_T^{jj} distributions between these two processes become much easier to figure out. When $60 \lesssim P_T^{jj} \lesssim 460$, the P_T^{jj} distributions of the process $e^+e^- \rightarrow q\bar{q}A'$ are significantly monotonic attenuated as P_T^{jj} increases. However, the P_T^{jj} distributions of the processes $e^+e^- \rightarrow q\bar{q}\phi$ increase quickly first and then decrease slowly in the same region. For a sound estimation, we also display the transverse momentum distributions of the background with same cuts, which show quite a different line shape from the signals at $\sqrt{s} = 91.2$ GeV.

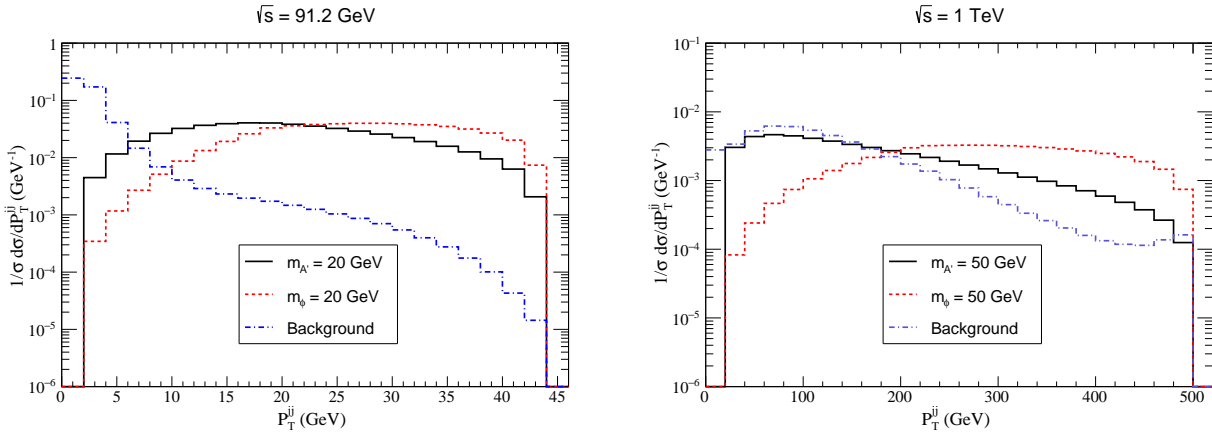


Figure 6: The normalized P_T^{jj} distributions of the two-jet system of the two signal processes and the background process at $\sqrt{s} = 91.2$ GeV (left panel) and 1 TeV (right panel), with cuts $-0.9 < \cos\theta_{jj-z} < 0.9$.

For the $\cos\theta_{jj-z}$ distributions in Fig. 7, we present the differential cross sections for those two signal processes at $\sqrt{s} = 91.2$ GeV, 240 GeV, 500 GeV, 1 TeV and $m_{A'}(m_\phi) = 20$ GeV or 50 GeV. It is found that the cuts on P_T^{jj} can enhance the difference between dark photon and dark scalar mediator production. By imposing the cuts of $P_T^{jj} > 20, 50, 100$ and 240 GeV for above four center-of-mass energy accordingly, we can find that the differential distributions for $e^+e^- \rightarrow q\bar{q}A'$ process reaches its maximum around $\cos\theta_{jj} = 0$, with a line shape of bottom-up “U”. However, for the scalar case, the maximum peak lies around $\cos\theta_{jj} = \pm 0.7$, and the line shape looks like character “M”. For angle distribution of the background with same cuts, we find that the line shapes vary dramatically with the four typical \sqrt{s} values.

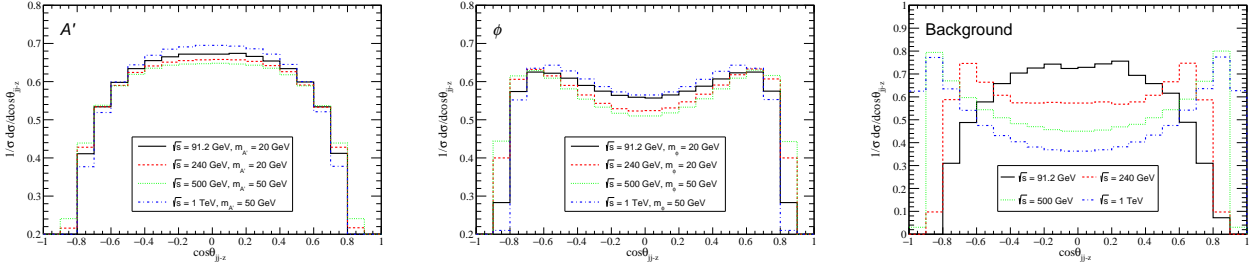


Figure 7: The normalized $\cos\theta_{jj}$ distributions of the two-jet system of the two signal processes and the background process at four different \sqrt{s} , with cuts $P_T^{jj} > 20, 50, 100$ and 240 GeV for $\sqrt{s} = 91.2$ GeV, 240 GeV, 500 GeV and 1 TeV, respectively.

4 Identify dark photon signals over the background

The future e^+e^- colliders might play a crucial role in discovering the nature of the DM (dark sector) particles since they have more clear background. In this section, we will focus on how to identify the heavy dark photon A' signals over the annoying background at future CEPC experiment. The analysis is similar for dark scalar mediator ϕ production at e^+e^- colliders. In the dark photon model with Eq. (1), A' can decay into SM quarks pair and DM pair. The related decay widths are defined as

$$\Gamma(A' \rightarrow \chi\bar{\chi}) = \frac{g_\chi^2(m_{A'}^2 + 2m_\chi^2)\sqrt{m_{A'}^2 - 4m_\chi^2}}{12\pi m_{A'}^2},$$

$$\sum_q \Gamma(A' \rightarrow q\bar{q}) = \sum_q \frac{\varepsilon^2 e^2 c_q^2 (m_{A'}^2 + 2m_q^2)\sqrt{m_{A'}^2 - 4m_q^2}}{4\pi m_{A'}^2}, \quad (5)$$

where c_q is the charge of the quarks. The branching ratio of $A' \rightarrow \chi\bar{\chi}$ can be written as

$$\text{Br}(A' \rightarrow \chi\bar{\chi}) = \frac{\Gamma(A' \rightarrow \chi\bar{\chi})}{\Gamma(A' \rightarrow \chi\bar{\chi}) + \sum_q \Gamma(A' \rightarrow q\bar{q})}, \quad (6)$$

which is related to g_χ and ε , while the combined parameter $\alpha_\chi \varepsilon^2$ can be obtained from the Fig.1. Here we choose $m_\chi = 8.6$ GeV, $g_\chi = 0.032$. We abstract ε from the XENON-1T curve in Fig. 1 and obtain the branching ratios of $A' \rightarrow \chi\bar{\chi}$ which are listed in Table. 1. In the following, we investigate the $e^+e^- \rightarrow q\bar{q}A'$ process with $A' \rightarrow \chi\bar{\chi}$ due to its cleaner background. Corresponding

$m_{A'}$	20 GeV	30 GeV	40 GeV	50 GeV	60 GeV
ε	0.0030	0.0067	0.012	0.019	0.027
$\text{Br}(A' \rightarrow \chi\bar{\chi})$	0.996	0.985	0.955	0.898	0.809

Table 1: Values of mixing parameter ε and branching ratios of $A' \rightarrow \chi\bar{\chi}$ with respect to dark photon mass $m_{A'}$, when m_χ is fixed at 8.6 GeV and g_χ is fixed at 0.032.

to this signal, the dominant background process is $e^+e^- \rightarrow q\bar{q}\nu\bar{\nu}$ ($\nu = \nu_e, \nu_\mu$, and ν_τ). In the final states of both signal and background processes, we observe only two jets. The background

process is simulated by MadGraph [59]. The invariant mass $M_{RA'}$ of the dark photon which can be reconstructed by recoiling the four-momentum of the two-jet system, where $M_{RA'}$ is defined as,

$$M_{RA'} = \sqrt{(p_{e^+} + p_{e^-} - p_{j1} - p_{j2})^2}, \quad (7)$$

where p_{e^+} , p_{e^-} , p_{j1} and p_{j2} are the four-momentum of the incoming electron, positron and the two jets in final states, respectively. Here, we focus on the light quark jets ($q = u, d, s, c$ and b) since the top quark decays quickly.

Theoretically, the on-shell dark photon events would be reconstructed precisely at $M_{RA'} = m_{A'}$ in the invariant mass spectrum. However, experimentally the detector has the restricted energy resolution, which results in some bump structures stretched in the $M_{RA'}$ spectrum. To make our estimate more realistic, we simulate this detector effect by smearing the jet energies according to the assumption of the Gaussian resolution parametrization,

$$\frac{\delta(E)}{E} = \frac{A}{\sqrt{E}} \oplus B, \quad (8)$$

where $\delta(E)/E$ is the energy resolution, A is a sampling term, B is a constant term and \oplus denotes a sum in quadrature. Following CEPC CDR [41], for light jets, the energy resolution ranges from 6% at $E = 20$ GeV to 3.6% at $E = 100$ GeV. We adopt the parameters $A = 25.7\%$ and $B = 2.4\%$. In the reconstruction of background events, the smearing effect is also considered in the same way.

In order to identify dark photon signals over the background, we need to impose proper kinematic cuts. The cuts are based on the kinematic distributions of both the signal and background processes. We set the basic transverse momentum cuts $P_T > 10$ GeV and rapidity cuts $|\eta_j| < 4$. In order to identify an isolated jet, the angular distribution between jets i and j is defined by

$$\Delta R_{ij} = \sqrt{\Delta\phi_{ij}^2 + \Delta\eta_{ij}^2}, \quad (9)$$

where $\Delta\phi_{ij}$ ($\Delta\eta_{ij}$) denotes the azimuthal angle (rapidity) difference between two jets. In our two-jet system, we set basic cut $\Delta R > 0.4$ for both signal and background processes.

In Fig. 8, we display the distribution of differential cross section $d\sigma/dM_{RA'}$ with respect to the invariant mass of dark photon with $m_{A'} = 20, 30, 40, 50$ and 60 GeV, within the smearing constrains under above kinematic cuts. These reconstructed signal bumps have the line shape complied with a Gaussian distribution with the expectation of $m_{A'}$ and standard deviation of the energy resolution values $\delta(E)$. In contrast to the $\sqrt{s} = 91.2$ GeV case, signal bumps at $\sqrt{s} = 240$ GeV have widen spread since $\delta(E)$ grows.

In order to identify dark photon signals over the background, one need to explore the significance or the signal-to-noise ratio. To enhance the significance, we impose the cut conditions on the invariant mass spectrum, i.e., $|M_{RA'} - m_{A'}| < 6$ GeV at $\sqrt{s} = 91.2$ GeV, and $|M_{RA'} - m_{A'}| < 12$ GeV at $\sqrt{s} = 240$ GeV. Running at $\sqrt{s} = 91.2$ GeV with integrated luminosity $\mathcal{L} = 2$ ab $^{-1}$ at CEPC, for several different $m_{A'}$ values, we estimate the number of events for both signal (N_S) and background (N_B) processes as well as the significance S/\sqrt{B} , as listed in Table 2. It is found that for $m_{A'} = 20, 30, 40$ and 50 GeV, the significance is greater than 3σ .

For the operating model with $\sqrt{s} = 240$ GeV at CEPC, we adopt a higher integrated luminosity of $\mathcal{L} = 20$ ab $^{-1}$. The events for signal and background processes as well as the significance S/\sqrt{B}

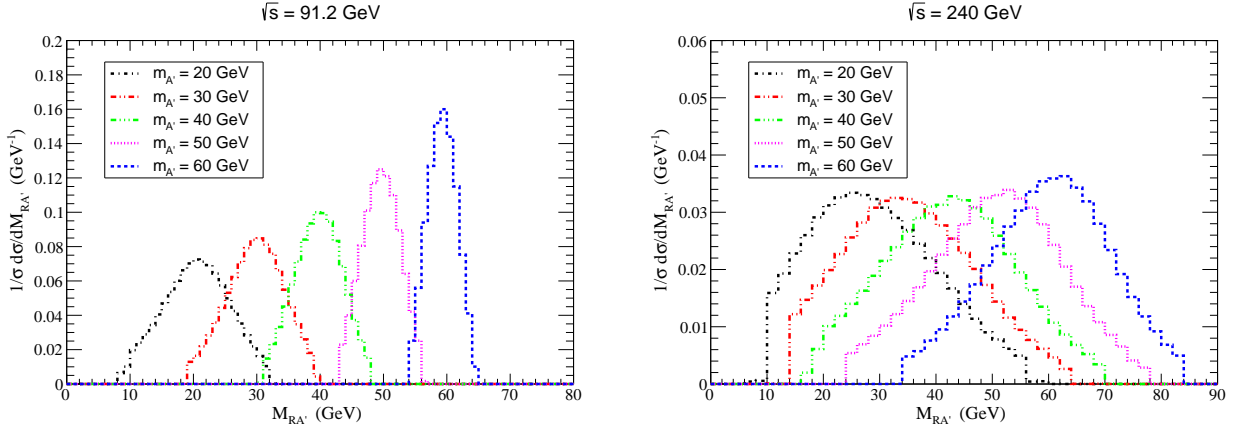


Figure 8: The normalized distributions of differential cross section $d\sigma/dM_{RA'}$ with respect to the invariant mass of dark photon with $m_{A'} = 20, 30, 40, 50$ and 60 GeV for the process $e^+e^- \rightarrow q\bar{q}A'$ at $\sqrt{s} = 91.2$ GeV (left panel) and $\sqrt{s} = 240$ GeV (right panel) within the smearing constraints under proper kinematic cuts.

$m_{A'}$	20 GeV	30 GeV	40 GeV	50 GeV	60 GeV
$N_S (\mathcal{L} = 2 \text{ ab}^{-1})$	191	368	372	206	46
$N_B (\mathcal{L} = 2 \text{ ab}^{-1})$	2503	3697	3636	2304	799
S/\sqrt{B}	3.82	6.05	6.17	4.29	1.63

Table 2: The number of events for both signal (N_S) and background (N_B) processes and the significance S/\sqrt{B} with integrated luminosity $\mathcal{L} = 2 \text{ ab}^{-1}$ at $\sqrt{s} = 91.2$ GeV, within the smearing constraints under proper kinematic cuts.

are given in Table 3. In comparison with Table 2, we obtain much less events of dark photon. This is understandable, for $20 \text{ GeV} < m_{A'} < 60 \text{ GeV}$, the cross section decreases with the increasement of the center-of-mass energy in $\sqrt{s} > 91.2$ GeV energy region, as demonstrated in Fig. 3 (a) and (c). In addition, we obtain much more background events at $\sqrt{s} = 240$ GeV than at $\sqrt{s} = 91.2$ GeV. This is due to the new topology of Feynman diagrams for background process like Fig. 9, whose contributions grow along with the increasing \sqrt{s} . This topology is excluded in the signal process since we assume the dark photon interacts only with quarks in our model.

$m_{A'}$	20 GeV	30 GeV	40 GeV	50 GeV	60 GeV
$N_S (\mathcal{L} = 20 \text{ ab}^{-1})$	2	10	23	39	53
$N_B (\mathcal{L} = 20 \text{ ab}^{-1})$	60252	114953	210674	380295	682870
S/\sqrt{B}	0.00815	0.0295	0.0501	0.0632	0.0641

Table 3: Same as Table 2 but with $\mathcal{L} = 20 \text{ ab}^{-1}$, $\sqrt{s} = 240$ GeV and $|M_{RA'} - m_{A'}| < 12$ GeV.

For a sound discussion at future CEPC experiment, we further present the significance S/\sqrt{B} versus the integrated luminosity at $\sqrt{s} = 91.2$ GeV and $\sqrt{s} = 240$ GeV in Fig. 10. For the case of $\sqrt{s} = 91.2$ GeV, the minimum integrated luminosities for 3σ discovery of the dark photon with $m_{A'} = 20, 30, 40, 50$ and 60 GeV are about 1.23, 0.490, 0.473, 0.971 and 6.67 ab^{-1} , respectively. So,

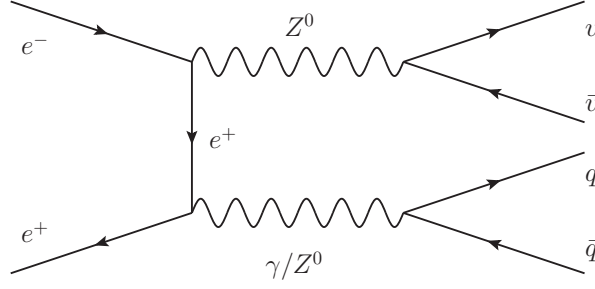


Figure 9: A possible topology of Feynman diagrams for background process, which is excluded for signal process.

it is understandable that no dark photon signals were found in the Large Electron-Positron (LEP) collider, since total luminosity of LEP experiment [60] does not reach the required minimum integrated luminosity for 3σ discovery of the dark photon with $20 \text{ GeV} < m_{A'} < 60 \text{ GeV}$. At CEPC with $\sqrt{s} = 91.2 \text{ GeV}$, the expected instantaneous luminosity would be $4 \text{ ab}^{-1}\text{year}^{-1}$ for single interaction point (CEPC will have two interaction points), thus it is possible for CEPC experiment to perform a decisive measurement on dark photon ($20 \text{ GeV} < m_{A'} < 60 \text{ GeV}$) in less than one operating year. For the case of $\sqrt{s} = 240 \text{ GeV}$, the minimum integrated luminosity to produce one signal event with above five $m_{A'}$ values are about 7.06, 1.91, 0.853, 0.508 and 0.374 ab^{-1} , respectively. However, running at $\sqrt{s} = 240 \text{ GeV}$ with luminosity of $0.4 \text{ ab}^{-1}\text{year}^{-1}$ for single interaction point, we could hardly find any signals of dark photon ($20 \text{ GeV} < m_{A'} < 60 \text{ GeV}$) in one operating year at CEPC.

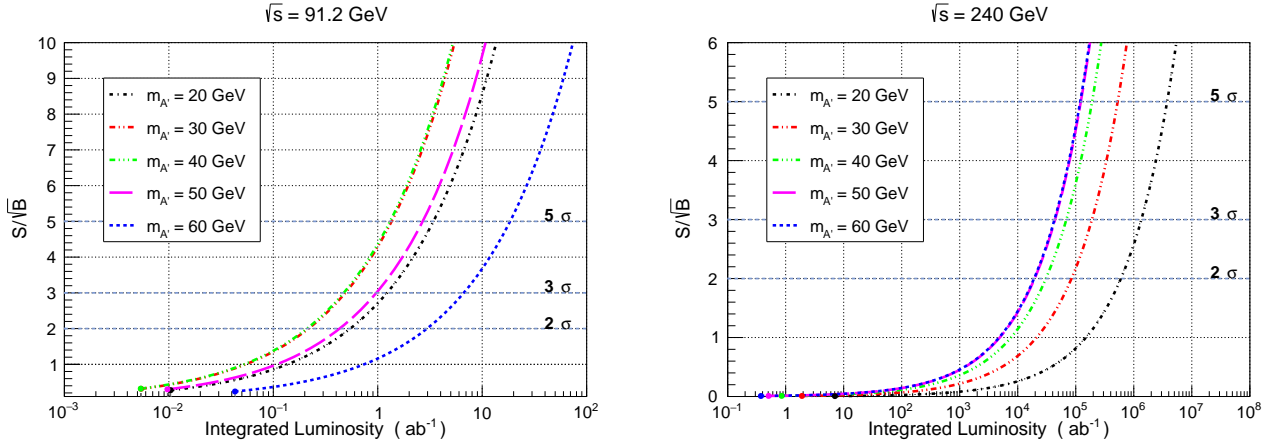


Figure 10: The plane of integrated luminosity and significance for $m_{A'} = 20, 30, 40, 50$ and 60 GeV at $\sqrt{s} = 91.2 \text{ GeV}$ (left panel) and $\sqrt{s} = 240 \text{ GeV}$ (right panel). The spots refer to the minimum integrated luminosity to produce one signal event.

5 Summary

The richer dark sector may consist of not only the DM itself but also one or more new force-carrying mediators which can couple to the SM particles. In this paper, we mainly discuss the

vector dark photon A' and the scalar mediator ϕ which can be produced via the processes of $e^+e^- \rightarrow q\bar{q}A'$ and $e^+e^- \rightarrow q\bar{q}\phi$ at future e^+e^- colliders. The production cross sections of the signal processes are predicted with $\sqrt{s} = 91.2$ GeV, 240 GeV, 500 GeV and 1 TeV. We further study the kinematic distributions of the two-jet system in final states in detail and find that they can be used to identify or exclude the dark photon and the dark scalar mediator, as well as distinguish between them. In this work, we only consider the interaction between dark photon and quarks, and take the process $e^+e^- \rightarrow q\bar{q}A'$ as an example, we investigate the discovery potential of the dark photon at CEPC with $\sqrt{s} = 91.2$ GeV and 240 GeV. It shows that the dark photon with $m_{A'}$ ranging from 20 GeV to 60 GeV might be discovered through the process $e^+e^- \rightarrow q\bar{q}A'$ at e^+e^- colliders, e.g., super-Z factory, CEPC, etc., with the minimum required integrated luminosity for 3σ discovery being about $0.473 \sim 6.67 \text{ ab}^{-1}$. If one also considers the interaction between dark mediator and leptons, $e^+e^- \rightarrow \ell^+\ell^-A'$ and $e^+e^- \rightarrow \gamma A'$ will be another interesting processes, and WW production is the corresponding background, which can be investigated further. The method proposed in this work can be used to search for any invisible particles in e^+e^- annihilation.

Acknowledgements

This work was supported in part by the National Natural Science Foundation of China (grant Nos. 11875179, 11325525, 11635009, 11775130 and 11905112), by the Natural Science Foundation of Shandong Province (grant Nos. ZR2017MA002, ZR2019QA012) and the Fundamental Research Funds of Shandong University (grant No. 2019GN038).

References

- [1] N. Aghanim *et al.* [Planck Collaboration], “Planck 2018 results. VI. Cosmological parameters,” arXiv:1807.06209 [astro-ph.CO].
- [2] C. Conroy, A. Loeb and D. Spergel, “Evidence Against Dark Matter Halos Surrounding the Globular Clusters MGC1 and NGC 2419,” *Astrophys. J.* **741**, 72 (2011), [arXiv:1010.5783 [astro-ph.GA]].
- [3] Y. Sofue and V. Rubin, “Rotation curves of spiral galaxies,” *Ann. Rev. Astron. Astrophys.* **39**, 137 (2001), [astro-ph/0010594].
- [4] S. Cole *et al.* [2dFGRS Collaboration], “The 2dF Galaxy Redshift Survey: Power-spectrum analysis of the final dataset and cosmological implications,” *Mon. Not. Roy. Astron. Soc.* **362**, 505 (2005), [astro-ph/0501174].
- [5] F. Beutler *et al.*, “The 6dF Galaxy Survey: Baryon Acoustic Oscillations and the Local Hubble Constant,” *Mon. Not. Roy. Astron. Soc.* **416**, 3017 (2011), [arXiv:1106.3366 [astro-ph.CO]].
- [6] L. Anderson *et al.*, “The clustering of galaxies in the SDSS-III Baryon Oscillation Spectroscopic Survey: Baryon Acoustic Oscillations in the Data Release 9 Spectroscopic Galaxy

- Sample,” *Mon. Not. Roy. Astron. Soc.* **427**, no. 4, 3435 (2013), [arXiv:1203.6594 [astro-ph.CO]].
- [7] A. Vikhlinin *et al.*, “Chandra Cluster Cosmology Project III: Cosmological Parameter Constraints,” *Astrophys. J.* **692**, 1060 (2009), [arXiv:0812.2720 [astro-ph]].
 - [8] L. Fu *et al.*, “Very weak lensing in the CFHTLS Wide: Cosmology from cosmic shear in the linear regime,” *Astron. Astrophys.* **479**, 9 (2008), [arXiv:0712.0884 [astro-ph]].
 - [9] R. Massey *et al.*, “COSMOS: 3D weak lensing and the growth of structure,” *Astrophys. J. Suppl.* **172**, 239 (2007), [astro-ph/0701480].
 - [10] G. Jungman, M. Kamionkowski and K. Griest, “Supersymmetric dark matter,” *Phys. Rept.* **267**, 195 (1996), [hep-ph/9506380].
 - [11] G. Bertone, D. Hooper and J. Silk, “Particle dark matter: Evidence, candidates and constraints,” *Phys. Rept.* **405**, 279 (2005), [hep-ph/0404175].
 - [12] T. Marrodñ Undagoitia and L. Rauch, “Dark matter direct-detection experiments,” *J. Phys. G* **43**, no. 1, 013001 (2016), [arXiv:1509.08767 [physics.ins-det]].
 - [13] J. M. Gaskins, “A review of indirect searches for particle dark matter,” *Contemp. Phys.* **57**, no. 4, 496 (2016), [arXiv:1604.00014 [astro-ph.HE]].
 - [14] F. Kahlhoefer, “Review of LHC Dark Matter Searches,” *Int. J. Mod. Phys. A* **32**, no. 13, 1730006 (2017), [arXiv:1702.02430 [hep-ph]].
 - [15] S. Tulin and H. B. Yu, “Dark Matter Self-interactions and Small Scale Structure,” *Phys. Rept.* **730**, 1 (2018), [arXiv:1705.02358 [hep-ph]].
 - [16] X. Chu, T. Hambye and M. H. G. Tytgat, “The Four Basic Ways of Creating Dark Matter Through a Portal,” *JCAP* **1205**, 034 (2012), [arXiv:1112.0493 [hep-ph]].
 - [17] J. A. Evans, S. Gori and J. Shelton, “Looking for the WIMP Next Door,” *JHEP* **1802**, 100 (2018) [arXiv:1712.03974 [hep-ph]].
 - [18] R. Essig *et al.*, “Working Group Report: New Light Weakly Coupled Particles,” arXiv:1311.0029 [hep-ph].
 - [19] J. Alexander *et al.*, “Dark Sectors 2016 Workshop: Community Report,” arXiv:1608.08632 [hep-ph].
 - [20] M. Pospelov, A. Ritz and M. B. Voloshin, “Secluded WIMP Dark Matter,” *Phys. Lett. B* **662**, 53 (2008) [arXiv:0711.4866 [hep-ph]].
 - [21] M. Dutra, M. Lindner, S. Profumo, F. S. Queiroz, W. Rodejohann and C. Siqueira, “MeV Dark Matter Complementarity and the Dark Photon Portal,” *JCAP* **1803**, 037 (2018), [arXiv:1801.05447 [hep-ph]].

- [22] B. Holdom, “Two U(1)’s and Epsilon Charge Shifts,” Phys. Lett. **166B**, 196 (1986).
- [23] M. Pospelov, “Secluded U(1) below the weak scale,” Phys. Rev. D **80**, 095002 (2009), [arXiv:0811.1030 [hep-ph]].
- [24] M. Cirelli, P. Panci, K. Petraki, F. Sala and M. Taoso, “Dark Matter’s secret liaisons: phenomenology of a dark U(1) sector with bound states,” JCAP **1705**, no. 05, 036 (2017), [arXiv:1612.07295 [hep-ph]].
- [25] S. N. Gninenko, D. V. Kirpichnikov, M. M. Kirsanov and N. V. Krasnikov, Phys. Lett. B **782**, 406 (2018) doi:10.1016/j.physletb.2018.05.010 [arXiv:1712.05706 [hep-ph]].
- [26] D. Banerjee *et al.* [NA64 Collaboration], Phys. Rev. D **97**, no. 7, 072002 (2018) doi:10.1103/PhysRevD.97.072002 [arXiv:1710.00971 [hep-ex]].
- [27] S. Abrahamyan *et al.* [APEX Collaboration], Phys. Rev. Lett. **107**, 191804 (2011) doi:10.1103/PhysRevLett.107.191804 [arXiv:1108.2750 [hep-ex]].
- [28] H. Merkel *et al.*, Phys. Rev. Lett. **112**, no. 22, 221802 (2014) doi:10.1103/PhysRevLett.112.221802 [arXiv:1404.5502 [hep-ex]].
- [29] A. Adare *et al.* [PHENIX Collaboration], Phys. Rev. C **91**, no. 3, 031901 (2015) doi:10.1103/PhysRevC.91.031901 [arXiv:1409.0851 [nucl-ex]].
- [30] J. L. Feng, I. Galon, F. Kling and S. Trojanowski, Phys. Rev. D **97**, no. 3, 035001 (2018) doi:10.1103/PhysRevD.97.035001 [arXiv:1708.09389 [hep-ph]].
- [31] P. Ilten, J. Thaler, M. Williams and W. Xue, Phys. Rev. D **92**, no. 11, 115017 (2015) doi:10.1103/PhysRevD.92.115017 [arXiv:1509.06765 [hep-ph]].
- [32] D. Curtin, R. Essig, S. Gori and J. Shelton, JHEP **1502**, 157 (2015) doi:10.1007/JHEP02(2015)157 [arXiv:1412.0018 [hep-ph]].
- [33] S. Chatrchyan *et al.* [CMS Collaboration], JHEP **1312**, 030 (2013) doi:10.1007/JHEP12(2013)030 [arXiv:1310.7291 [hep-ex]].
- [34] J. P. Lees *et al.* [BaBar Collaboration], Phys. Rev. Lett. **119**, no. 13, 131804 (2017) doi:10.1103/PhysRevLett.119.131804 [arXiv:1702.03327 [hep-ex]].
- [35] P. Fayet, Phys. Rev. D **75**, 115017 (2007) doi:10.1103/PhysRevD.75.115017 [hep-ph/0702176 [HEP-PH]].
- [36] M. He, X. G. He, C. K. Huang and G. Li, JHEP **1803**, 139 (2018) doi:10.1007/JHEP03(2018)139 [arXiv:1712.09095 [hep-ph]].
- [37] J. Jiang, H. Yang and C. F. Qiao, Eur. Phys. J. C **79**, no. 5, 404 (2019) doi:10.1140/epjc/s10052-019-6912-3 [arXiv:1810.05790 [hep-ph]].

- [38] A. Anastasi *et al.* [KLOE-2 Collaboration], Phys. Lett. B **757**, 356 (2016) doi:10.1016/j.physletb.2016.04.019 [arXiv:1603.06086 [hep-ex]].
- [39] P. Ilten, Y. Soreq, J. Thaler, M. Williams and W. Xue, “Proposed Inclusive Dark Photon Search at LHCb,” Phys. Rev. Lett. **116**, no. 25, 251803 (2016), [arXiv:1603.08926 [hep-ph]].
- [40] V. Prasad [BESIII Collaboration], “Dark matter/new physics searches at BESIII,” arXiv:1907.12058 [hep-ex].
- [41] J. B. Guimarães da Costa *et al.* [CEPC Study Group], arXiv:1811.10545 [hep-ex].
- [42] H. Baer *et al.*, “The International Linear Collider Technical Design Report - Volume 2: Physics,” arXiv:1306.6352 [hep-ph].
- [43] M. Bicer *et al.* [TLEP Design Study Working Group], “First Look at the Physics Case of TLEP,” JHEP **1401**, 164 (2014), [arXiv:1308.6176 [hep-ex]].
- [44] H. Abramowicz *et al.* [CLIC Detector and Physics Study Collaboration], “Physics at the CLIC e^+e^- Linear Collider – Input to the Snowmass process 2013,” arXiv:1307.5288 [hep-ex].
- [45] N. Fornengo, P. Panci and M. Regis, “Long-Range Forces in Direct Dark Matter Searches,” Phys. Rev. D **84**, 115002 (2011), [arXiv:1108.4661 [hep-ph]].
- [46] M. Kaplinghat, S. Tulin and H. B. Yu, “Direct Detection Portals for Self-interacting Dark Matter,” Phys. Rev. D **89**, no. 3, 035009 (2014), [arXiv:1310.7945 [hep-ph]].
- [47] R. H. Helm, “Inelastic and Elastic Scattering of 187-MeV Electrons from Selected Even-Even Nuclei,” Phys. Rev. **104**, 1466 (1956).
- [48] J. D. Lewin and P. F. Smith, “Review of mathematics, numerical factors, and corrections for dark matter experiments based on elastic nuclear recoil,” Astropart. Phys. **6**, 87 (1996).
- [49] C. Y. Li, Z. G. Si and Y. F. Zhou, “Constraints on dark matter interactions from the first results of DarkSide-50,” Nucl. Phys. B **945**, 114678 (2019), [arXiv:1904.02193 [hep-ph]].
- [50] T. Li, S. Miao and Y. F. Zhou, “Light mediators in dark matter direct detections,” JCAP **1503**, 032 (2015), [arXiv:1412.6220 [hep-ph]].
- [51] R. Agnese *et al.* [CDMS Collaboration], “Silicon Detector Dark Matter Results from the Final Exposure of CDMS II,” Phys. Rev. Lett. **111**, no. 25, 251301 (2013), [arXiv:1304.4279 [hep-ex]].
- [52] H. Jiang *et al.* [CDEX Collaboration], “Limits on Light Weakly Interacting Massive Particles from the First 102.8 kg \times day Data of the CDEX-10 Experiment,” Phys. Rev. Lett. **120**, no. 24, 241301 (2018), [arXiv:1802.09016 [hep-ex]].
- [53] A. Tan *et al.* [PandaX-II Collaboration], “Dark Matter Results from First 98.7 Days of Data from the PandaX-II Experiment,” Phys. Rev. Lett. **117**, no. 12, 121303 (2016), [arXiv:1607.07400 [hep-ex]].

- [54] P. Agnes *et al.* [DarkSide Collaboration], “Low-Mass Dark Matter Search with the DarkSide-50 Experiment,” *Phys. Rev. Lett.* **121**, no. 8, 081307 (2018), [arXiv:1802.06994 [astro-ph.HE]].
- [55] E. Aprile *et al.* [XENON Collaboration], “Dark Matter Search Results from a One Ton-Year Exposure of XENON1T,” *Phys. Rev. Lett.* **121**, no. 11, 111302 (2018), [arXiv:1805.12562 [astro-ph.CO]].
- [56] T. Hahn, “Generating Feynman diagrams and amplitudes with FeynArts 3,” *Comput. Phys. Commun.* **140**, 418 (2001), [hep-ph/0012260].
- [57] V. Shtabovenko, R. Mertig and F. Orellana, “New Developments in FeynCalc 9.0,” *Comput. Phys. Commun.* **207**, 432 (2016), [arXiv:1601.01167 [hep-ph]].
- [58] T. Hahn, “Concurrent Cuba,” *Comput. Phys. Commun.* **207**, 341 (2016).
- [59] J. Alwall *et al.*, “The automated computation of tree-level and next-to-leading order differential cross sections, and their matching to parton shower simulations,” *JHEP* **1407**, 079 (2014), [arXiv:1405.0301 [hep-ph]].
- [60] S. Schael *et al.* [ALEPH and DELPHI and L3 and OPAL and SLD Collaborations and LEP Electroweak Working Group and SLD Electroweak Group and SLD Heavy Flavour Group], “Precision electroweak measurements on the Z resonance,” *Phys. Rept.* **427**, 257 (2006), [hep-ex/0509008].